Synthesis and Evaluation of High-Performance Ethylene–Propylene–Diene Terpolymer/Organoclay Nanoscale Composites

H. Acharya,[1] M. Pramanik,[1] S. K. Srivastava,[1] A. K. Bhowmick[2]

[1]*Department of Chemistry, Indian Institute of Technology, Kharagpur 721302, India*
[2]*Rubber Technology Centre, Indian Institute of Technology, Kharagpur 721302, India*

Received 19 December 2003; accepted 23 March 2004
DOI 10.1002/app.20774
Published online in Wiley InterScience (www.interscience.wiley.com).

ABSTRACT: The main objective of this study was to synthesize and characterize the properties of ethylene–propylene–diene terpolymer (EPDM)/clay nanocomposites. Pristine clay, sodium montmorillonite (Na^+–MMT), was intercalated with hexadecyl ammonium ion to form modified organoclay (16Me–MMT) and the effect of intercalation toward the change in interlayer spacing of the silicate layers was studied by X-ray diffraction, which showed that the increase in interlayer spacing in Na^+–MMT by 0.61 nm is attributed to the intercalation of hexadecyl ammonium ion within the clay layers. In the case of EPDM/16Me–MMT nanocomposites, the basal reflection peak was shifted toward a higher angle. However, gallery height remained more or less the same for different EPDM nanocomposites with organoclay content up to 8 wt %. The nanostructure of EPDM/clay composites was characterized by transmission electron microscopy, which established the coexistence of intercalated and exfoliated clay layers with an average layer thickness in the nanometer range within the EPDM matrix. The significant improvement in thermal stability and mechanical properties reflects the high-performance nanocomposite formation. © 2004 Wiley Periodicals, Inc. J Appl Polym Sci 93: 2429–2436, 2004

Key words: nanocomposites; TEM; clay; ethylene–propylene–diene terpolymer (EPDM); morphology

INTRODUCTION

Polymer/clay mineral nanocomposites, a fascinating class of materials, have assumed considerable importance in recent years and have been the focus of extensive investigations.[1–11] This is mainly attributed to the nanoscale dimension of silicate layers dispersed in the polymer matrix, which causes a strong interfacial interaction between silicate layers and polymer chains, leading to a dramatic change in the thermal stability behavior, mechanical, dynamic mechanical, barrier and optical properties, and fire resistance compared to properties of pristine polymer.[12–18] In most of the polymer/clay nanocomposites reported so far, clay minerals have been widely used as reinforcing agents of choice because of their cheapness and easy availability[14,19,20] compared to other layered materials.[21–23] Specifically, naturally occurring sodium montmorillonite (Na^+–MMT), belonging to the phyllosilicate family (2 : 1), is customarily used. The crystal lattice of Na^+–MMT consists of a central octahedral sheet of alumina/magnesium sandwiched between two fused tetrahedral sheets. The isomorphic substitution Si^{4+} by Al^{3+} and Al^{3+} by Mg^{2+} or Fe^{2+} makes the pristine clay layer negatively charged, which is counterbalanced by the hydrated cations (Li^+, Na^+, Rb^+, Cs^+, Ca^{2+}) in the interlayer gallery.[24–26]

The inorganic backbone of the hydrophilic Na^+–MMT is rendered organophilic by treatment with aliphatic alkylammonium or alkyl phosphonium cations. This replacement of hydrated metal ions from interlayer space by organic cation plays a synergistic role by balancing the negative charges and modifying the clay from hydrophilic to hydrophobic. Such an organomodification of clay results in diminishing the surface energy, making the silicate layers compatible with organic polymers.[4,15] It appears that the repulsive interaction between the two negatively charged adjacent silicate layers may play an important role in allowing the positively charged organic ammonium ion between them. When the organomodified clay is dispersed within a polymer matrix, the polymer–organic ammonium ion interaction is attractive and simultaneously the effective interaction between the clay layers becomes repulsive, which favors the insertion of polymer chains between the silicate layers.[27,28] The influence of organomodified clay toward the various

Correspondence to: S. K. Srivastava (sunil111954@yahoo.co.uk).

Contract grant sponsor: Council of Scientific and Industrial Research (CSIR), India.
Contract grant sponsor: Ministry of Human Research and Development (MHRD), India.

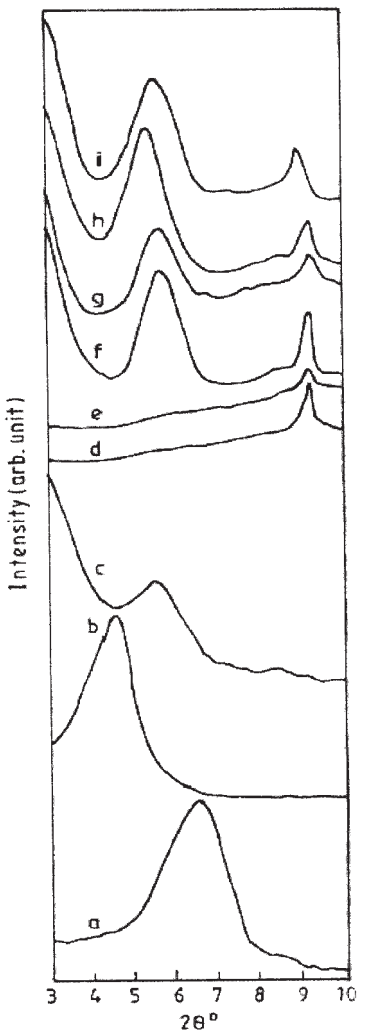

Figure 1 X-ray diffractograms of (a) Na^+–MMT, (b) 16Me–MMT, (c) treated 16Me–MMT, (d) EPDM, (e) EPDM + 2 wt % 16Me–MMT, (f) EPDM + 3 wt % 16Me–MMT, (g) EPDM + 4 wt % 16Me–MMT, (h) EPDM + 6 wt % 16Me–MMT, and (i) EPDM + 8 wt % 16Me–MMT.

properties of different polymers has been studied extensively, with some studies on rubber–clay nanocomposites.[10,29,30] In our earlier work on ethylene vinyl acetate (EVA)/clay nanocomposites[3,31–33] it was observed that the EVA matrix is substantially reinforced, both mechanically and thermally, in the presence of 4–6 wt % organomodified Na^+–MMT.

Ethylene–propylene–diene terpolymer (EPDM) is one of the most widely used and fastest growing synthetic rubbers because of its excellent resistance to heat, oxidation, ozone, weathering, and microbial attack, attributed to the stable and saturated polymer backbone structure. Because of these unique features, it finds applications in automotive weather-stripping and seals, radiator, electrical insulation, roofing membrane, tubing, belts, and other general-purpose applications, which dominate its impact with regard to various industrial aspects. This motivated us to develop nanocomposites based on EPDM.[34,35] Therefore, a primary aim of the present work was to prepare high-performing EPDM/16Me–MMT nanocomposites by solution blending. These composites were characterized by X-ray diffraction, transmission electron microscopy (TEM), scanning electron microscopy (SEM), and FTIR spectroscopy and were evaluated in terms of mechanical properties and thermal stability behavior.

EXPERIMENTAL

Materials

Sodium montmorillonite (Na^+–MMT, SWy1), with a cation-exchange capacity of 76.4 meq/100 g was received from the clay mineral repository of University of Missouri (Columbia, MO). Hexadecyl amine was obtained from SRL Pvt. Ltd. (Mumbai, India). EPDM terpolymer (Keltan 520), containing different monomers [Mooney viscosity of 46 $ML_{(1+4)}$ at 125°C; density 0.86 g/mL; ethylene content 58 wt %], was received from DSM (Galeen, The Netherlands). Hydrochloric acid was purchased from E. Merck Ltd. (Mumbai, India). Dicumyl peroxide (DCP), from Hercules, Inc. (Gibbstown, NJ), was used as the crosslinking agent.

Preparation of organophilic clay and its nanocomposites with epdm

Sodium montmorillonite was dispersed homogeneously in hot water. A mixture of hexadecyl amine and concentrated hydrochloric acid was dissolved in hot water to obtain a solution of hexadecyl ammonium chloride salt. This solution was then added to the hot dispersion of montmorillonite, under vigorous stirring using a homogenizer, and stirring was continued for about 1 h to yield a large mass of white precipitate. The white precipitate thus obtained was filtered and washed with hot water to make it chloride

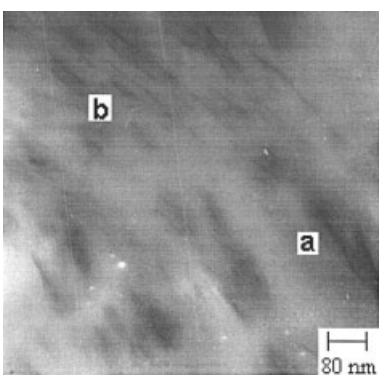

Figure 2 Transmission electron microphotograph of nanocomposite containing 8 wt % 16Me–MMT in EPDM matrix.

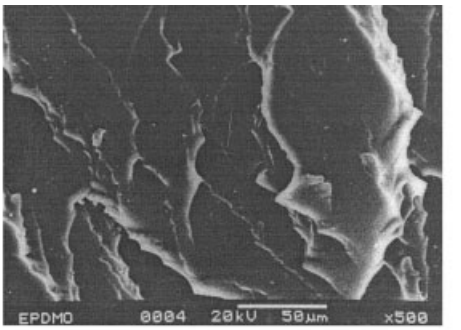

(a)

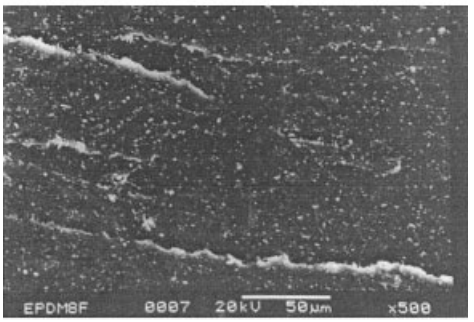

(b)

Figure 3 Scanning electron microphotographs of fracture surfaces of (a) EPDM and (b) nanocomposite containing 8 wt % 16Me–MMT in EPDM matrix.

free. The product was dried under vacuum and ground and sieved through a 270-mesh size sieve. This product was designated as 16Me–MMT.

EPDM/clay composites having different weight percentages of organomodified clay (16Me–MMT) were prepared by a solution blending method. An appropriate amount of hydrophobic organoclay dispersion was added to the solution of EPDM rubber in toluene, with vigorous stirring under hot condition. After 2 h, dicumyl peroxide was added as catalyst to promote crosslinking and afterward the solvent was extracted under reduced pressure. The resultant composites were compression molded by a hydraulically operated press at 150°C for 45 min.

Characterization techniques

X-ray diffraction (XRD) studies were performed by using a Miniflex diffractometer (30 kV, 10 mA; Rigaku Corp., Tokyo, Japan) with Cu–K_α radiation in the 2θ range 3–10° at a scanning range of 2°/min at room temperature. FTIR spectra of Na^+–MMT, 16Me–MMT, EPDM, and 16Me–MMT/EPDM composites were obtained by using a Nexus 870 FTIR spectrometer (Nicolet Analytical Instruments, Madison, WI) over a frequency range from 400 to 4000cm^{-1}. The dispersion of organophilic clay in the EPDM matrix and the nanostructure were observed through microscopic investigations on a JEM 3010 high-resolution transmission electron microscope (TEM; JEOL, Tokyo, Japan). Scanning electron microscopic (SEM) photographs of the EPDM/16Me–MMT hybrids were observed on a JEOL JSM-5800 with an acceleration voltage of 20 kV. The mechanical properties were measured in a Zwick (Ulm, Germany) model 1445 according to ASTM standard D 412-97 at an extension rate of 500 mm/min. Thermogravimetric analysis of virgin EPDM and its composites was carried out on a TG 209 (Netzsch-Gerätebau GmbH, Bavaria, Germany), at a heating rate of 20°C/min over a temperature range from 30 to 800°C in air atmosphere.

RESULTS AND DISCUSSION

XRD analysis

XRD patterns of the Na^+–MMT, 16Me–MMT, pure EPDM, and 16Me–MMT/EPDM hybrids are displayed in Figure 1. This shows that when the clay is treated with hexadecyl ammonium ions, the 001 basal reflection peak of Na^+–MMT located at $2\theta = 6.5°$ ($d_{001} = 1.35$ nm) is shifted to 4.5° ($d_{001} = 1.96$ nm), leading to an increase in the gallery height by 0.61 nm. Pure EPDM does not exhibit any peak in this region. An almost similar XRD pattern is observed in the case of its composite containing 2 wt % of organoclay. This is probably attributable to the complete exfoliation of silicate layers in the EPDM matrix. Alternatively, the possibility of detection of such a small amount of organophilic clay (2 wt %) is also limited by the XRD instrument. Interestingly, with an increase in organophilic clay loading in the EPDM matrix a peak appears at around $2\theta = 5.5°$. This clearly shows that at higher filler loading, intercalation predominates over exfoliation because of the aggregating tendency of silicate

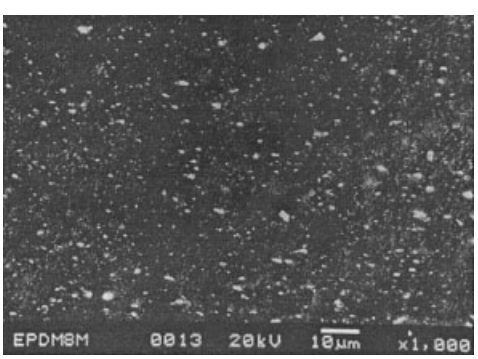

Figure 4 Scanning electron microphotograph of nanocomposite containing 8 wt % 16Me–MMT in EPDM matrix.

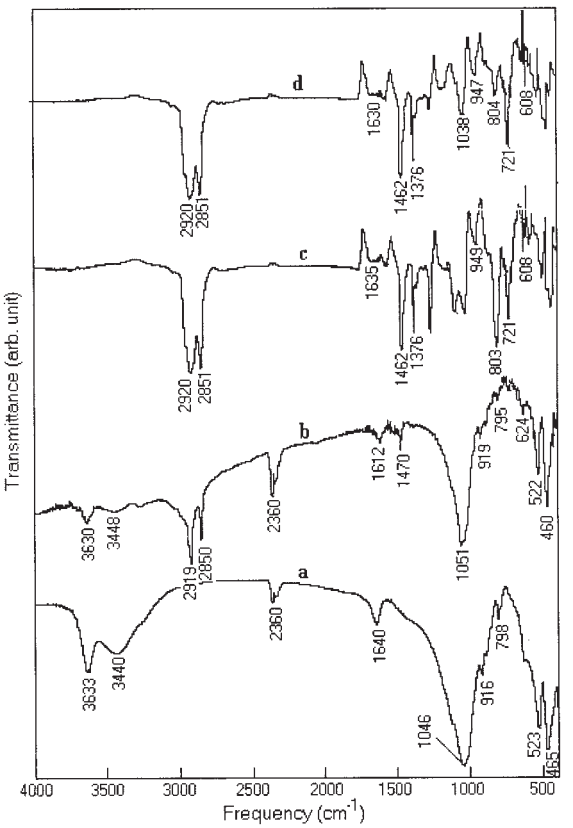

Figure 5 FTIR spectra of (a) Na^+–MMT, (b) 16Me–MMT, (c) EPDM, and (d) EPDM + 4 wt % 16Me–MMT.

layers. In addition, a shift of basal reflection peak from $2\theta = 4.5$ to 5.5° of organophilic clay in the EPDM matrix is observed, which demonstrates the compression of the silicate gallery height. Such a decrease in *d*-spacing of silicate layers of MMT dispersed in the EPDM matrix could be attributed to the partial decomposition of the hexadecyl ammonium and expulsion of the ammonium salt during preparation under thermal condition, leading to the collapse of the organoclay interlayer distance.[36–39] XRD of the organomodified 16Me–MMT, treated at 150°C for 45 min, was taken and is displayed in Figure 1(c), which shows that the basal reflection peak is shifted from $2\theta = 4.5°$ to $2\theta = 5.5°$, which confirmed our earlier view.

TEM studies

Figure 2 shows the TEM image of EPDM/organoclay composite containing 8 wt % 16Me–MMT, which depicts the presence of intercalated clay tactoids with a partial exfoliation of silicate layers marked as (a) and (b) portions, respectively. Earlier works on polymer–clay nanocomposites[11,15,39] also confirm our observations that the intercalated as well as exfoliated silicate layers coexist together. It is also clearly observed from Figure 2 that the average size of the silicate layers dispersed in the EPDM matrix is in the range of 15–20 nm.

SEM studies

SEM images of nanocomposites are very informative with respect to their fracture surface morphology and the distribution of silicate layers in the polymer matrix. Such observations on fracture surfaces of pure EPDM and 8 wt % 16Me–MMT/EPDM nanocomposites are displayed in Figure 3(a) and (b), respectively. In the absence of filler, the fracture surface of neat EPDM shows a characteristic cross-hatched morphological pattern, which is composed of numerous webs and steps of different sizes. The fracture surface image of 16Me–MMT/EPDM nanocomposite distinctly reveals the appearance of a typical line-flow pattern, which is absent in neat EPDM. This typical line flow is generally observed if the layered aggregates resulting from the intercalation are dispersed at a regular interval across the thickness of the rubber sheet and the cracks pass through along the edges of the aggregates. It may be noted that nitrile butadiene rubber (NBR) and NBR/clay nanocomposites also exhibit a cross-hatched pattern and typical line flow pattern morphology, respectively.[40] SEM images displayed in Figure 4 shows the segregation of the silicate layers of organomodified clay in the EPDM matrix indicating the homogeneous distribution of clay layers in the EPDM matrix.

TABLE I
Assignment of Important Bands of FTIR Spectra

Observed band (cm^{-1})	Band assignment
3633, 3630	O—H stretching of hydroxyl group
3440	O—H stretching of water
3448	N—H stretching of ammonium ion
2920, 2919	C—H asymmetric stretching of CH_2 or CH_3
2850, 2851	C—H symmetric stretching of CH_2 or CH_3
2360, 2342	CO_2 gaseous
1640	O—H deformation of water
1635	C═C stretching (unconjugated)
1612, 1611	N—H bending
1470, 1462	C—H (CH_2) scissoring and C—H (CH_3) asymmetric bending
1376	C—H (CH_3) symmetric bending
1051, 1046, 1038	Si—O stretching
949, 947	C—H (CH_2) rocking
919, 915	Al—O—H stretching
804, 803	═C—H bending
797, 795	Si—O—Si asymmetric stretching
726, 721	CH_2 rocking
522, 521	Al—O—Si deformation
464, 459	Si—O—Si deformation

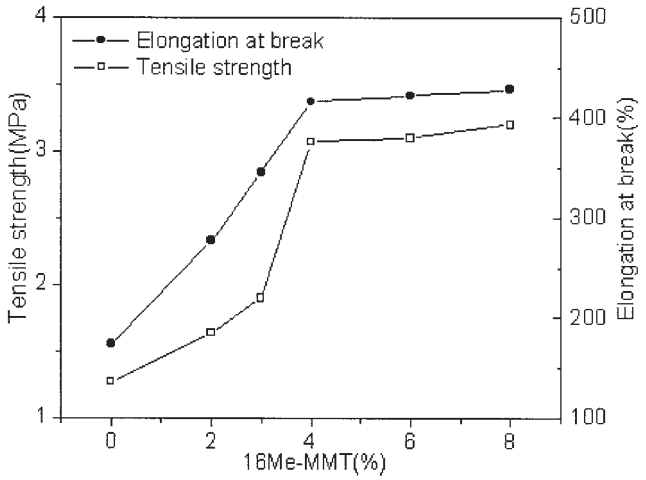

Figure 6 Variation of tensile strength and elongation at break versus 16Me–MMT content.

FTIR studies

Figure 5 shows the precise FTIR spectra of Na^+–MMT, 16Me–MMT, EPDM, and its nanocomposites with 16Me–MMT. The important bands of all the samples are assigned in Table I. Na^+–MMT exhibits characteristic bands at around 3633, 3440, 1640, 1046, 522, and 464 cm^{-1}, attributed to the –OH stretching of structural hydroxyl groups, –OH stretching of water, –OH deformation of water, Si—O stretching, Al—O—Si deformation, and Si—O—Si deformation, respectively.[3,41] A few new bands appear at 2919, 2850, and 3448 cm^{-1}, attributed to C—H asymmetric and C—H symmetric stretching of CH_2 or CH_3 and N—H stretching, respectively,[42] supporting the intercalation of hexadecyl ammonium ion within the clay layers. The peak at 1470 cm^{-1} is attributed to asymmetric bending of C—H of alkyl ammonium ion in 16Me–MMT. The notable frequency band at 1635 cm^{-1} is attributed to unconjugated C═C stretching, indicating the presence of the characteristic band of EPDM.[43] A band at 721 cm^{-1} is assigned to the rocking-mode vibration, attributed to the presence of a longer methylene sequence in EPDM chains. In addition to this, the bands in the range of 1000–650 cm^{-1} are attributed to the out-of-plane ═C—H bending in EPDM. The Si—O stretching band in EPDM/16Me–MMT nanocomposites appears at around 1038 cm^{-1}. The band related to N—H bending appears at 1612 and 1611 cm^{-1}, attributed to the alkyl ammonium ion in 16Me–MMT and in 16Me–MMT/EPDM composites, respectively. It is also noted that the characteristic bands assigned to the $–CH_3$ group in toluene, in the range of 1800–2000 cm^{-1}, are absent, thus suggesting that no more solvent, used as medium for the development of EPDM nanocomposites, is entrapped within the polymer matrix.

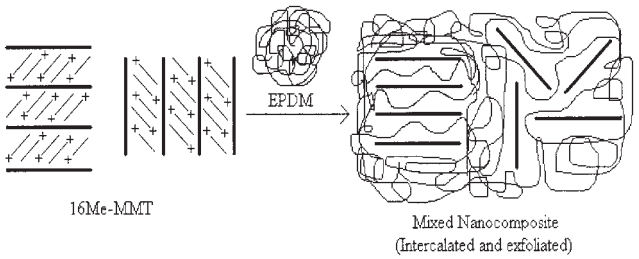

Scheme 1 A very short sketch of mixed nanocomposite along with entanglement of polymer chains.

Mechanical properties

The reinforcement in mechanical properties of 16Me–MMT/EPDM nanocomposites with increasing clay content is clarified with the tensile test. Figure 6 represents the effect of silicate layers on the tensile strength (TS) and elongation at break (EB). This indicates that TS and EB both increase sharply with 16Me–MMT contents up to 4 wt % and the corresponding improvement in either case is about 2.4 times with respect to that of the neat EPDM. Such an unusual improvement in TS is ascribed to the strong interfacial interaction between silicate layers and polymer chains. The noteworthy improvement in EB may be attributable to the extensive entanglement of the crosslinkable EPDM chains, which are surrounded by dispersed clay layers, as shown in Scheme 1. On further incorporation of 16Me–MMT in EPDM, both the TS and EB remain almost identical, compared to 4 wt % filler, which indicates that the aggregation tendency of the clay layers in the EPDM matrix gradually dominates. It may be mentioned that the mechanical properties also depend on the amount of the inhomogeneous weak spots in the rubber.[29] Data in Table II represent the influence of 16Me–MMT on modulus at different elongations of EPDM. From tensile testing it is observed that the pure EPDM breaks below 200% elongation and its nanocomposite, containing 2 wt % 16Me–MMT, breaks below 300% elongation. Therefore it appears that the strength of neat EPDM is too low to

TABLE II
Modulus at Different Elongations of EPDM and Its Nanocomposites

Sample	Modulus (MPa) at the elongation (%) of		
	100%	200%	300%
Pure EPDM	0.92	—	—
EPDM + 2 wt % 16Me–MMT	0.95	1.18	—
EPDM + 3 wt % 16Me–MMT	0.97	1.32	1.73
EPDM + 4 wt % 16Me–MMT	1.05	1.63	2.24
EPDM + 6 wt % 16Me–MMT	1.09	1.75	2.35
EPDM + 8 wt % 16Me–MMT	1.15	1.82	2.43

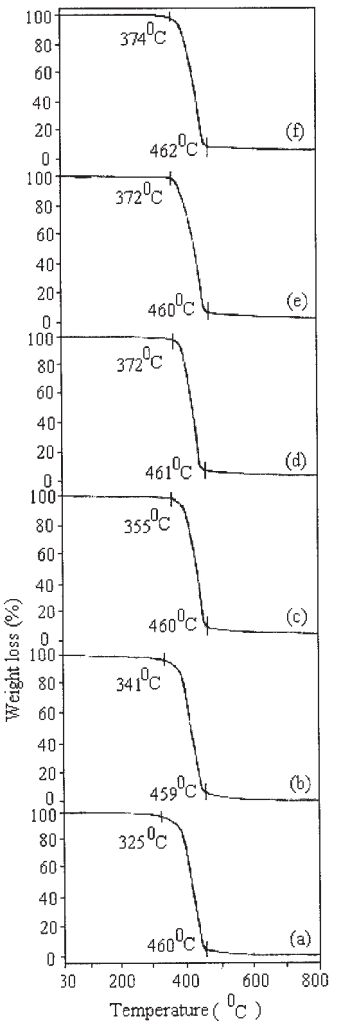

Figure 7 TGA of (a) EPDM, (b) EPDM + 2 wt % 16Me–MMT, (c) EPDM + 3 wt % 16Me–MMT, (d) EPDM + 4 wt % 16Me–MMT, (e) EPDM + 6 wt % 16Me–MMT, (f) EPDM + 8 wt % 16Me–MMT nanocomposites.

attain 200% elongation. Similar is the case with 2 wt % 16Me–MMT filler containing EPDM nanocomposite, which also shows a mechanical failure below 300%. Because of this, the respective modulus values are not provided in Table II. It is seen that modulus increases with increasing 16Me–MMT content in EPDM in all cases. Such an increase in modulus of 16Me–MMT/EPDM nanocomposites is attributed either to the resistance exerted by the sterically hindered organophilic 16Me–MMT surface itself or to the possibility of a strong polymer–filler interaction originating from each intercalated and exfoliated layer.[39]

Thermogravimetric analysis

Figure 7 shows a typical nonisothermal weight loss curve resulting from the thermal degradation of EPDM and its 16Me–MMT nanocomposites. It shows a very sharp one-step weight loss, in all cases corresponding to the thermal degradation of the unsaturated organic backbone accompanied by the main chain scission on oxidation.[15] The thermal stability behavior corresponding to initial thermal decomposition temperature (T_i) for 2 wt % loss in mass improves from 325 to 374°C for neat EPDM to 8 wt % 16Me–MMT content EPDM nanocomposites, successively. This significant improvement in thermal stability is more likely attributable to the presence of silicate layers, offering a great barrier effect to hinder the formation of small molecules, resulting from thermal decomposition, and simultaneously resisting their movement during desorption from the surface.[44,45] The coexistence of intercalated and exfoliated silicate layers in the EPDM matrix, which increases the (Si—O—C) interfacial interaction to restrict the thermal motion of EPDM polymer segments, is another possibility that further strengthens our earlier view.[46] Furthermore, it is noteworthy that the final thermal decomposition temperature (T_f) at about 460°C remains more or less the same irrespective of the presence of 16Me–MMT in EPDM. It appears that the final T_f of EPDM is no longer dependent on the effect of silicate layers, suggesting their incapability of holding the polymer chains within themselves.[41] Data relating the comparison in thermal stability behavior of virgin EPDM and EPDM nanocomposites, having 2, 3, 4, 6, and 8 wt % 16Me–MMT as filler, are presented in Table III.

TABLE III
Thermal Stability Behavior of Pure EPDM and Its Nanocomposites

Sample	Initial thermal decomposition temperature, T_i (°C)	Final decomposition temperature, T_f (°C)	Weight loss (%)
Pure EPDM	325	460	96.4
EPDM + 2 wt % 16Me–MMT	341	459	95.2
EPDM + 3 wt % 16Me–MMT	355	460	92.2
EPDM + 4 wt % 16Me–MMT	372	461	92.1
EPDM + 6 wt % 16Me–MMT	372	460	92.0
EPDM + 8 wt % 16Me–MMT	374	462	91.8

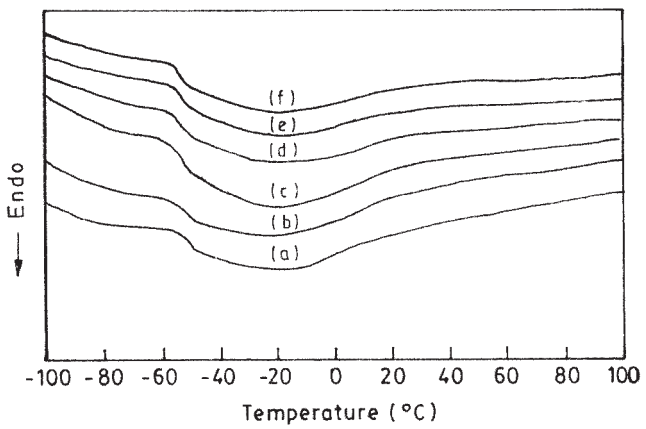

Figure 8 Differential scanning calorimetric curve of (a) EPDM, (b) EPDM + 2 wt % 16Me–MMT, (c) EPDM + 3 wt % 16Me–MMT, (d) EPDM + 4 wt % 16Me–MMT, (e) EPDM + 6 wt % 16Me–MMT, and (f) EPDM + 8 wt % 16Me–MMT nanocomposites.

Differential scanning calorimetric (DSC) analysis

DSC analysis of EPDM and its nanocomposites, with different weight percentages of 16Me–MMT filler, is displayed in Figure 8, which shows a decreasing trend in endothermic transition, with respect to glass-transition temperature (T_g), from −51°C (neat EPDM) to −53°C (8 wt % 16Me–MMT/EPDM). Such a decrease in T_g, although not significant, in all probability is attributable to the reduction in cohesive forces of attraction between polymer chains. The reduction in cohesive forces originates when the silicate layers, which are relatively smaller in size compared to the polymer molecules, penetrate into the polymer matrix and establish polar attractive forces between silicate layers and chain segments of the polymer. This, in turn, reduces the cohesive forces between polymer chains and simultaneously increases segmental mobility, thus leading to a decrease in T_g, which further supports the formation of the nanocomposite.[47]

CONCLUSIONS

Ethylene–propylene–diene terpolymer (EPDM)/clay nanocomposites were successfully prepared by blending hexadecyl ammonium ion intercalated montmorillonite (16Me–MMT) with EPDM in solution. X-ray diffraction and TEM studies confirmed the formation of intercalated as well as exfoliated configuration of 16Me–MMT/EPDM nanocomposites. The average layer thickness of organomodified clay in EPDM matrix is in the nanometer range. The successive improvement in mechanical properties of 16Me–MMT/EPDM nanocomposites with increasing 16Me–MMT content from 2 to 8 wt % was observed. For example, the tensile strength of the EPDM/organoclay nanocomposite, containing 8 wt % 16Me–MMT, is about 2.5 times higher than that of the neat EPDM. Thermal stability was also significantly improved for 16Me–MMT/EPDM nanocomposites over that of the pure EPDM. Thus, it can be finally concluded that the nanocomposite of EPDM with organophilic clay (16Me–MMT), prepared by a solution blending method, attains superior performance in terms of mechanical and thermal properties over those of conventional composites.

The authors are grateful to Council of Scientific and Industrial Research (CSIR) and Ministry of Human Research and Development (MHRD) for the financial support to carry out this investigation.

References

1. Giannelis, E. P. Adv Mater 1996, 8, 29.
2. Lagaly, G.; Pinnavaia, T. J. Appl Clay Sci 1999, 15, 303.
3. Pramanik, M.; Srivastava, S. K.; Samantaray, B. K.; Bhowmick, A. K. J Mater Sci Lett 2001, 20, 1717.
4. Pinnavaia, T. J; Beall, G. W. Polymer–Clay Nanocomposites (Wiley Series in Polymer Science); Wiley: New York, 2000.
5. Kim, D. W.; Blumstein, A.; Kumar, J.; Tripathy, S. K. K. Chem Mater 2001, 13, 243.
6. Biswas, M.; SinhaRay, S. Polymer 1998, 39, 6423.
7. Giannelis, E. P.; Krishnamoorti, R.; Manias, E. Adv Polym Sci 1999, 138, 108.
8. Kojima, Y.; Usuki, A.; Kawasumi, M.; Okada, A.; Kurauchi, T. Lunigato, O. J. J Polym Sci Part A: Polym Chem 1993, 31, 983.
9. Hasegawa, N.; Okamoto, H.; Kato, M.; Usuki, A. J Appl Polym Sci 2000, 78, 1981.
10. Ray, S.; Bhowmick, A. K. Radiat Phys Chem 2002, 65, 259.
11. Manias, E.; Touny, A.; Wu, L.; Strawhecker, K.; Lu, B.; Chung, T. C. Chem Mater 2001, 13, 3516.
12. Krishnamoorti, R.; Giannelis, E. P. Macromolecules 1997, 30, 4097.
13. Zanetti, M.; Lomakin. S.; Camino, G. Macromol Mater Eng 2000, 279, 1.
14. Ray, S.; Bhowmick, A. K. Rubber Chem Technol 2001, 74, 835.
15. Alexandre, M.; Dubosis, P. Mater Sci Eng 2001, R-28, 1.
16. Hasegawa, N.; Kawasumi, M.; Kato, M.; Usuki, A.; Okada, A. J Appl Polym Sci 1998, 67, 87.
17. Boogh, L.; Pettersson, B.; Manson, J. A. E. Polymer 1999, 40, 2249.
18. Okamato, M.; Nam, P. H.; Maiti, P.; Kotaka, T.; Nakayama, T.; Takada, M.; Oshina, M.; Usuki, A.; Hasegawa, N.; Okamato, H. Nano Lett 2001, 1, 503.
19. Theng, B. K. G. Formation and Properties of Clay–Polymer Complexes; Elsevier: Amsterdam, 1979.
20. Arroyo, M.; Lopez-Machado, M. A.; Herrero, B. Polymer 2000, 43, 3699.
21. Levy, F. Crystallography and Crystal Chemistry of Materials with Layered Structures, Vol. 2; Reidel: Dordrecht, 1976.
22. Benavente, E.; Santa Ana, M. A.; Mendizabal, F.; Gonzalez, G. Coord Chem Rev 2002, 224, 87.
23. Srivastava, S. K.; Pramanik, M.; Palit, D.; Mathur, B. K.; Kar, A. K.; Samantaray, B. K.; Haeuseler, H.; Cordes, W. Chem Mater 2001, 13, 4342.
24. Pinnavaia, T. J. Science 1983, 220, 365.
25. Bala, P.; Samantaray, B. K.; Srivastava, S. K.; Haeuseler, H. Z Kristallogr 2000, 215, 235.
26. Bala, P.; Samantaray, B. K.; Srivastava, S. K. Mater Res Bull 2000, 35, 1717.
27. Vaia, R. A.; Giannelis, E. P. Macromolecules 1997, 30, 8000.

28. Nam, P. H.; Maiti, P.; Okamoto, M.; Kotaka, T.; Hasegawa, N.; Usuki, A. Polymer 2001, 42, 9633.
29. Arroyo, M.; Lopez-Manchado, M. A.; Herrero, B. Polymer 2003, 44, 2447.
30. Usuki, A.; Tukigase, A.; Kato, M. Polymer 2002, 43, 2185.
31. Pramanik, M.; Srivastava, S. K.; Samantaray, B. K.; Bhowmick, A. K. J Polym Sci Part B: Polym Phys 2002, 40, 2065.
32. Pramanik, M.; Srivastava, S. K.; Samantaray, B. K.; Bhowmick, A. K. J Appl Polym Sci 2002, 87, 2216.
33. Pramanik, M.; Srivastava, S. K.; Samantaray, B. K.; Bhowmick, A. K. Macromol Res 2003, 11, 260.
34. Karger-Kocsis, J.; Kallo, A.; Szafner, A.; Bodor, G.; Senyei, Z. S. Polymer 1979, 20, 37.
35. Bhowmick, A. K.; Stephens, H. L. Handbook of Elastomers, 2nd ed.; Marcel Dekker: New York, 2001.
36. Heinemann, J.; Reichert, P.; Thomann, R.; Mulhaupt, R. Macromol Rapid Commun 1999, 20, 423.
37. Zanetti, M.; Camino, G.; Thomann, R.; Mulhaupt, R. Polymer 2001, 42, 4501.
38. Jones, M., Jr. Organic Chemistry, 2nd ed.; Norton: New York, 2000; p. 258.
39. Zanetti, M.; Camino, G.; Canavese, D.; Morgan, A. B.; Lamelas, F. J.; Wilkie, C. A. Chem Mater 2002, 14, 189.
40. Nah, C.; Ryu, H. J.; Han, S. H.; Rhee, J. M.; Lee, M. H. Polym Int 2001, 50, 1265.
41. Noh, M. H.; Jang, L. W.; Lee, D. C. J Appl Polym Sci 1999, 74, 179.
42. Shen, Z.; Simon, G. P.; Cheng, Y. B. Polymer 2002, 43, 4251.
43. Barra, G. M. O.; Crespo, J. S.; Bertolino, J. R.; Soldi, V.; Pires, A. T. J. Braz Chem Soc 1999, 10, 31.
44. Gilman, J. W.; Kashivagi, T. C. L.; Giannelis, E. P.; Manias, E.; Lomakin, S.; Lichtenhan, J. D.; Jones, P.; In: Fire Retardancy of Polymers; LeBras, M.; Camino, G.; Bourbigot, S.; Delobel, R., Eds.; The Royal Society of Chemistry: Cambridge, UK, 1998.
45. Wang, Z.; Pinnavaia, T. J. Chem Mater 1998, 10, 1820.
46. Chang, J. H.; Park, D. K. Polym Bull 2001, 47, 191.
47. Lee, S. S.; Lee, C. S.; Kim, M. H.; Kwak, S. Y.; Park, M.; Lim, S.; Choe, C. R.; Kim, J. J Polym Sci Part B: Polym Phys 2001, 39, 2430.